Jurnal Teknologi

Full Paper

MICROWAVE REFLECTOMETRY CIRCUITS INTEGRATION WITH COAXIAL PROBE FOR INITIAL BREAST TUMOR DETECTION

Kok Yeow You[a]*, Nadera Najib Al-Areqi[a], Wei Jer Lim[b], Kim Yee Lee[c], Ee Meng Cheng[d], Cheng Seong Khe[e],

[a]Faculty of Electrical Engineering, Universiti Teknologi Malaysia, UTM, 81310 UTM Johor Bahru, Johor, Malaysia
[b]Department of Electrical and Electronic Engineering, Southern University College, 81300 Skudai, Johor, Malaysia
[c]Lee Kong Chian Faculty of Engineering and Science, Universiti Tunku Abdul Rahman, 43200 Kajang, Selangor, Malaysia
[d]Faculty of Electronic Engineering and Technology, Universiti Malaysia Perlis, 02600 Arau, Perlis, Malaysia
[e]Fundamental and Applied Sciences Department, Universiti Teknologi PETRONAS, 32610 Perak, Seri Iskandar, Malaysia

Article history
Received
16 May 2024
Received in revised form
1 June 2024
Accepted
9 July 2024
Published Online
22 December 2024

*Corresponding author
kyyou@fke.utm.my

Graphical abstract

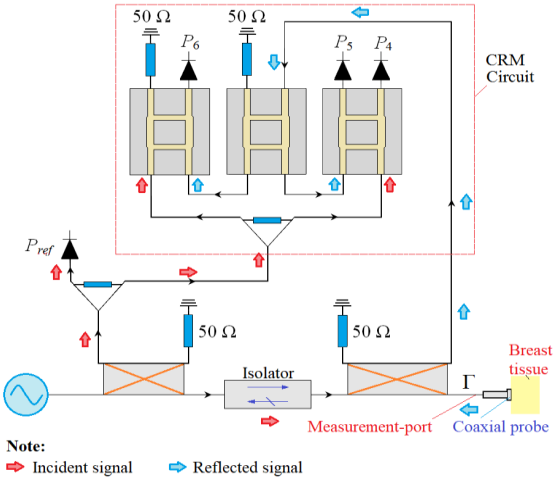

Abstract

A six-port reflectometry (SPR) system was developed to predict the dielectric properties of both tumor and normal breast tissue, intended for medical diagnostic applications. Ensuring precise measurements, the SPR underwent calibration using a well-established four-step procedure, which will be briefly outlined. Afterward, the investigated coaxial probe was connected to the SPR through the calibrated measurement port. Subsequently, the exposed end of the probe aperture was immersed into synthetic samples representing both healthy and cancerous breast tissue to assess the dielectric constant, ε_r' and loss factor, ε_r'' across frequencies ranging from 1.5 GHz to 3.3 GHz. The dielectric constant, ε_r' and loss factor, ε_r'' were derived from the measured reflection coefficient using a closed-form equation associated with the coaxial probe. An examination was undertaken to compare the performance of a commercially available vector network analyzer (VNA) outfitted with a Keysight 85070E dielectric probe against an SPR-probe system. The comparison was based on analyzing the reflection coefficient magnitude, phase shift, dielectric constant, and loss factor of synthetic breast tissue samples. The study revealed maximum absolute errors of 0.01, 1.07°, 1.12, and 0.75 for the measured reflection coefficient magnitude, phase shift, dielectric constant, and loss factor, respectively. The calibrated reflection coefficient and predicted relative permittivity, ε_r can be effectively utilized to distinguish between normal ($\varepsilon_r' < 50$) and tumor ($\varepsilon_r' > 50$) breast tissue.

Keywords: Complex-ratio-measuring circuits, synthetic breast tumors, one-port calibration, relative complex permittivity, open-ended coaxial probe, reflection coefficient

Abstrak

Sistem reflekometri enam port (SPR) telah dibangunkan untuk meramalkan sifat-sifat dielektrik bagi kedua-dua tumor dan tisu payudara normal untuk tujuan applikasi diagnostik perubatan. Untuk memastikan pengukuran yang tepat, SPR telah ditentukur menggunakan prosedur empat langkah yang mantap. Selepas itu, probe sepaksi yang dikaji disambungkan kepada SPR di port pengukuran yang ditentukur. Hujung terbuka apertur probe tersebut kemudiannya direndam secara berasingan ke dalam sampel sintetik tisu payudara normal dan tumor untuk mengukur pemalar dielektrik, ε_r' dan faktor kehilangan, ε_r'' merentasi julat frekuensi dari 1.5 GHz hingga 3.3 GHz. Pemalar dielektrik, $\varepsilon r'$ dan faktor kehilangan, ε_r'' diperoleh daripada pekali pantulan yang diukur melalui persamaan bentuk pendekatan untuk probe sepaksi. Kajian perbandingan telah dijalankan antara penganalisis rangkaian vektor komersial (VNA) yang dilengkapi dengan probe dielektrik Keysight 85070E dan sistem probe-SPR berdasarkan magnitud pekali pantulan, anjakan fasa pekali pantulan, pemalar dielektrik, dan faktor kehilangan sampel tisu payudara sintetik yang diukur. Dalam kajian ini, ralat mutlak maksimum bagi magnitud pekali pantulan yang diukur, anjakan fasa, pemalar dielektrik, dan faktor kehilangan didapati masing-masing adalah 0.01, 1.07°, 1.12, dan 0.75. Pekali pantulan yang ditentukur dan kebolehtelusan relatif, εr yang diramalkan dapat digunakan secara berkesan untuk membezakan antara tisu payudara normal ($\varepsilon_r' < 50$) dan tumor ($\varepsilon_r' > 50$).

Kata kunci: Litar-pengukur-nisbah-kompleks, tumor payudara sintetik, penentukuran satu-port, kebolehtelusan kompleks relatif, probe sepaksi hujung terbuka, pekali pantulan

1.0 INTRODUCTION

Breast cancer, identified by the World Health Organization (WHO) as a leading cancer affecting women globally, claimed estimated 2.001 million women have female breast cancer and 611,720 deaths in the United States in 2024 [1]. The decline in cancer mortality is projected to persist annually until 2021, resulting in the prevention of over 4 million deaths since 1991 [1]. Advanced early detection techniques for particular types of cancers, coupled with enhanced treatment options for both adjuvant and metastatic stages, play significant roles in improving outcomes. Consequently, the development of reliable diagnostic instruments is pivotal.

The manuscript aims to propose the creation of a simple, portable breast diagnostic device suitable for clinics and households alike, with affordability as a key consideration. Recently, microwave technology offers promise, with two modalities, namely microwave tomography and radar - showing potential [2, 3, 4]. The tissue with water content demonstrates a notable reaction attributed to the polarization of water molecules upon exposure to microwave radiation. However, existing instruments like vector network analyzers (VNA) pose drawbacks in terms of size and cost.

This study introduces a multi-port reflectometer (SPR) as an alternative to Vector Network Analyzers (VNAs) for measuring relative complex permittivity, ε_r in breast tissue [5]. The characterization of biological matter using microwaves typically involves the measurement of relative complex permittivity, ε_r ($= \varepsilon_r' - j\varepsilon_r''$) [6]. Differences in ε_r between normal and cancerous tissues are instrumental in diagnosis, as tumor tissues typically display higher water content (>60%) due to increased hydration from rapid cancer cell metabolism. The dielectric constant, ε_r' plays a crucial role in distinguishing between normal ($\varepsilon_r' < 50$ at 2.45 GHz) and cancerous ($\varepsilon_r' > 50$ at 2.45 GHz) tissue, offering a diagnostic indicator for cancer detection based on ε_r values [7, 8, 9, 10, 11, 12, 13, 14]. Consequently, the sensitivity of the SPR-sensor system to water content, influenced by tumor metabolism, contributes significantly to tumor detection.

Over the past fifty years, various types of multi-port reflectometry circuits have been developed, including three-port/four-port, five-port ring-based, and six-port/seven-port configurations. While three- and four-port circuits are simple and economical, they are normally limited to single or narrowband applications. Five-port circuits provide enhanced bandwidth, albeit at the expense of reduced phase stability and port isolation when compared to circuits with six or seven ports. Although seven-port circuits have slightly better isolation and phase stability, the simplicity and cost-effectiveness of six-port circuits make them preferable for this study. In this study, a comprehensive and concise description of the internal flow signal calibration process for the six-port circuit is provided.

The coaxial probes are widely used for dielectric measurements of breast tissue due to their simplicity, non-destructiveness, and ability to cover a wide operating frequency [3, 7, 8, 9, 10, 11, 12, 13, 14, 15, 16, 17]. For instance, recently, Canicattì *et al*. (2023) conducted clinical testing using a coaxial probe on real breast biopsy tissues, including both healthy and unhealthy samples. The study found that the coaxial probe achieved a sensitivity of 81.6%, a specificity of 61.5%, and an accuracy of 73.4% in the early detection of breast cancer, compared to conventional histological evaluation [15].

However, commercial dielectric probes are prohibitively expensive [9, 10, 11, 12, 13, 14, 16, 17]. Therefore, in this study, a common and extremely low-cost SMA connector is modified for use as a sensor probe in breast dielectric measurement applications. The use probe is machined from the jack flange mount SMA connector achieves a compact and cost-effective solution. The probe's effective sensing volume is analyzed using simulation results. In addition, a simple probe aperture calibration method is proposed, requiring only one calibration standard: the open (air) standard. This method aims to reduce complexity and time consumption in the calibration process compared to the conventional method, which typically requires three calibration standards.

While many studies measuring the dielectric properties of breast tissue use custom coaxial probes connected to costly commercial VNAs [8, 9, 10, 11, 12, 13, 14, 15, 16, 17], this study differs from previous studies by offering a comprehensive approach. It includes the development of a six-port vector reflectometer and the customization and implementation of coaxial probe specifically for dielectric measurements. In Malaysia, conducting clinical trials involving real human tissues entails navigating complex administrative processes, adhering to strict protocol conditions, and incurring significant insurance/maintenance costs. Therefore, this study is limited to *in vitro* reflection and dielectric measurements using synthetic breast tissue samples.

2.0 METHODOLOGY

2.1 Six-Port Complex-Ratio-Measuring Circuit

The primary elements within a six-port complex-ratio-measuring (CRM) network consist of three hybrid couplers and one power divider, depicted in Figure 1. To enhance the bandwidth and reduce the size of the CRM circuit, a customized three-section branch-line coupler and 3 dB-Wilkinson power dividers with optimized series-diamond stubs and meandering lines are employed, as illustrated in Figure 2 [18, 19]. The modified Wilkinson power divider [18] and the study six-port CRM circuit [19] are capable of operating across the frequency spectrum from 1.5 GHz to 3.3 GHz.

The complete prototype of the integrated six-port reflectometer (SPR) sensor system is depicted in Figure 3, comprises not only the CRM circuit component but also incorporates several key elements. These include the Keysight N5171B RF analog signal generator, a modified Wilkinson power divider [18], two units of Pasternack PE2243-10 10-dB directional couplers, four units of Herotek DZR124AAP Schottky diodes, an ICS-4749 wideband isolator, a coaxial probe, and various digital elements, such as four units of 24-bit LTC2400 analogue-to-digital converters (ADCs), an Arduino Nano microcontroller, four units of ADA-4528 chopper amplifiers, and a computer.

Utilizing a reverse connection of two 10-dB directional couplers proves more effective in enhancing the isolation between incident and reflected signals compared to employing a single bidirectional coupler. Further enhancement in isolation performance is achieved by integrating an isolator between the two directional couplers. The DZR124AAP Schottky diodes are passive detectors with a typical minimum detectable power limit of -30 dBm. Therefore, it is recommended that the signal generator output a power level of +15 dBm. To further enhance the detected power, chopper amplifiers are added to the output of each detector. A 24-bit ADC is employed to ensure a low signal-to-noise ratio (S/N) for the detected signal, enabling a dynamic range for reflection coefficient measurements of over 30 dB. An Arduino Nano microcontroller is used to control and extract the detected power values at each port. Given its compatibility with MATLAB software, a MATLAB-based graphical user interface (GUI) is created to facilitate communication between the Arduino microcontroller and a personal computer (PC), as shown in Figure 4.

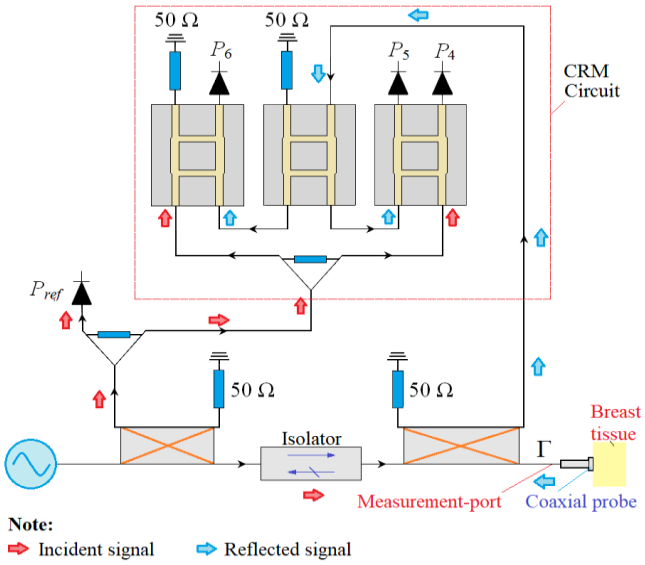

Figure 1 Six-port CRM circuit

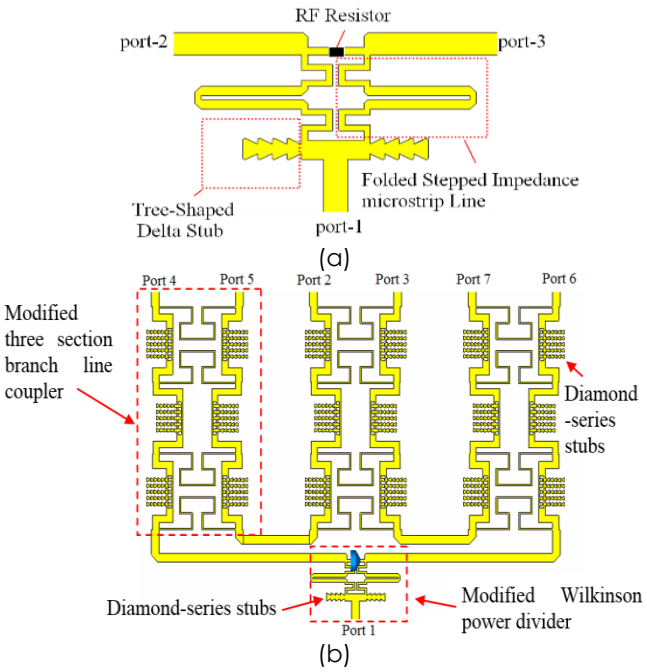

Figure 2 (a) Modified Wilkinson Power divider part [14]. (b) Six-port CRM circuit [15]

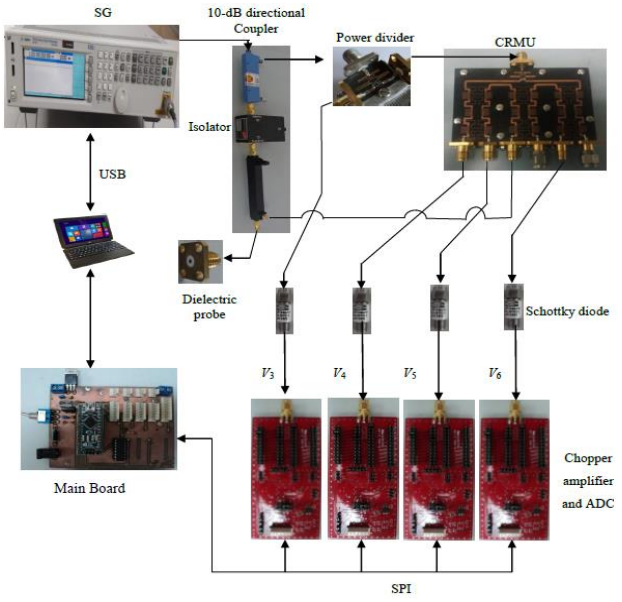

Figure 3 Six-port reflectometer (SPR) probe sensor system

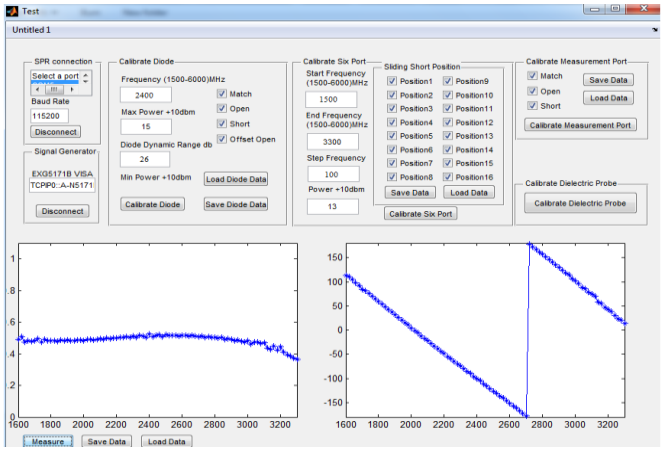

Figure 4 GUI for SPR-probe sensor system

2.2 Coaxial Probe

In order to cater to the minimal amount of breast tissue samples required for measurement, a cost-effective SMA connector with a small stub radius is adapted into a coaxial probe for the measurements. The stub of the SMA connector is removed, and the cut surface is carefully polished until achieving a uniformly smooth surface, as shown in Figure 5. The fabricated coaxial probe features inner and outer conductor radii of a = 0.635 mm and b = 2.05 mm, respectively, as depicted in Figures 6(a) and (b). The dielectric medium filling the space between the inner and outer conductors is Teflon, with a dielectric constant, ε_c of 2.06. Additionally, the physical length of the coaxial line, d from the connector end to the aperture probe is measured at 7.6 mm, as illustrated in Figure 6(c). This d value holds significant importance for converting the reflection coefficient, Γ at the measurement port to the aperture probe.

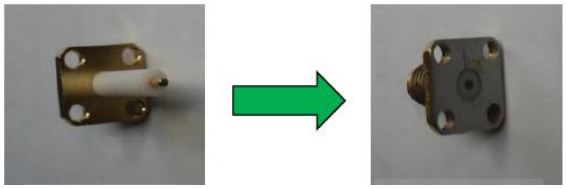

Figure 5 (a) SMA stub panel connector (b) fabricated coaxial probe

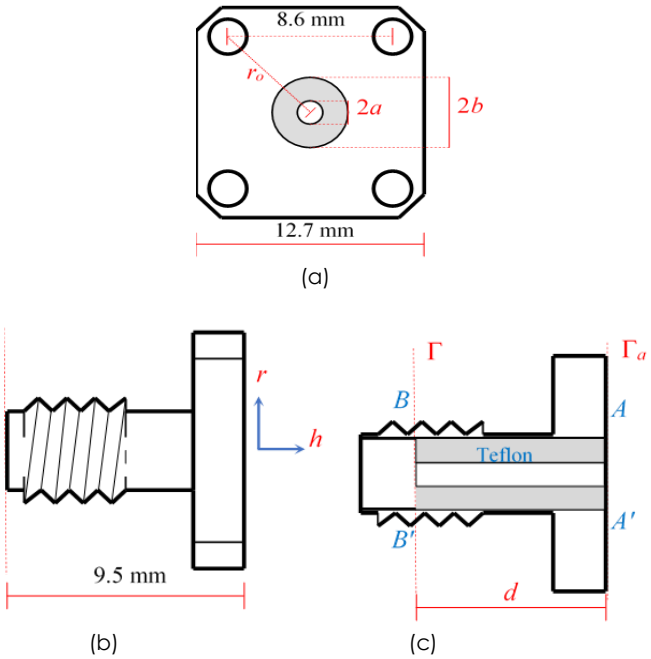

Figure 6 (a) Front view, (b) side view, and (c) cross-sectional view of the fabricated coaxial probe

The sensing distance, h from probe aperture is specified by simulated results obtained from COMSOL Multiphysics simulator as shown in Figure 7. The sensing distance, h can be estimated based on distance at which the simulated aperture complex reflection coefficient, Γ_a (linear magnitude, $|\Gamma_a|$ and phase shift, ϕ_a) becomes constant as the metal plate is gradually shifted away from the aperture probe in four kinds of samples with relative complex permittivity, ε_r of $51 - j9$, $38 - j8.5$, $24 - j7.5$, and $4.4 - j1.55$, respectively (See Figure 8). In fact, the four kind of samples correspond to tumour and normal breast tissues (will discuss in Section 'Synthetic Breast Tissues'). Overall, when the metal plate from aperture probe exceeds 4 mm (equal to diameter of outer conductor, $2b$), the simulated phase shift, ϕ_a at 2.45 GHz is constant with h. Although the $|\Gamma_a|$ of the samples (especially the samples with high dielectric constant value) still varies with h when it exceeds 4 mm, it is not very significant.

The effect of aperture flange on leaky of the sensor signal is also studied through simulation results. The magnetic field, H_ϕ of all four samples along the probe radius, r at the probe aperture are simulated as shown in Figure 9. It is found that the field of H_ϕ decreases sharply when it passes the radius distance of $r = b$. The field of H_ϕ decreases to near zero when r exceeds 6 mm. Thus, the influence of the four holes on the flanges at $r = r_o = 6$ mm on the leakage of the sensing signal is negligible. The percentage relative error (%) in the prediction of ε_r, which is derived from reflection coefficient, Γ_a, can be analyzed as [20]:

$$\left|\frac{\Delta\varepsilon_r}{\varepsilon_r}\right| = \frac{1}{S}\left|\frac{\Delta\Gamma_a}{\Gamma_a}\right| \times 100\% \quad (1)$$

where S is the sensitivity coefficient which can be determined as [20]:

$$S = \left| -\varepsilon_r \left(\frac{Y_o + j\omega\varepsilon_r C_o}{Y_o - j\omega\varepsilon_r C_o} \right) \left[\frac{2j\omega C_o}{Y_o \left(1 + \frac{j\omega\varepsilon_r C_o}{Y_o} \right)^2} \right] \right| \quad (2)$$

Symbol $Y_o = [(2\pi)/\ln(b/a)]\sqrt{(\varepsilon_o\varepsilon_c/\mu_o\mu_r)}$, and ω are the characteristic admittance and the angular frequency. The ε_o (= 8.8541878×10^{-12} F/m) and μ_o (= 1.2566371×10^{-6} H·m^{-1}) represent the free-space permittivity and permeability, respectively. The aperture probe capacitance, C_o is found based on the simulated aperture reflection coefficient, Γ_{a_Air} of air through:

$$C_o = \left(\frac{Y_o}{j\omega} \right) \left(\frac{1 - \Gamma_{a\_Air}}{1 + \Gamma_{a\_Air}} \right) \quad (3)$$

Utilizing equations (1) and (2), the relative change in the reflection coefficient, $|\Delta\Gamma_a/\Gamma_a|$ with respect to the relative change in relative complex permittivity, $|\Delta\varepsilon_r/\varepsilon_r|$ for four kinds of samples at 2.45 GHz, can be predicted and tabulated in Table 1. In this error analysis, the relative error, $|\Delta\Gamma_a/\Gamma_a|$ in reflection coefficient measurement is assumed to be 1%, 5%, and 10%, respectively.

Table 1 The influences of $|\Delta\Gamma_a/\Gamma_a|$ on $|\Delta\varepsilon_r/\varepsilon_r|$ for four samples at 2.45 GHz

Sample	$\lvert\Delta\Gamma_a/\Gamma_a\rvert$ (%)	$\lvert S\rvert$	$\lvert\Delta\varepsilon_r/\varepsilon_r\rvert$ (%)
$\varepsilon_r = 4.4 - j1.55$	1	0.2093	4.78
	5	0.2093	23.89
	10	0.2093	47.78
$\varepsilon_r = 24 - j7.5$	1	0.8893	1.12
	5	0.8893	5.62
	10	0.8893	11.24
$\varepsilon_r = 38 - j8.5$	1	1.0161	0.98
	5	1.0161	4.92
	10	1.0161	9.84
$\varepsilon_r = 51 - j9$	1	1.0024	1.00
	5	1.0024	4.99
	10	1.0024	9.98

The small percentage changes in $|\Delta\Gamma_a/\Gamma_a|$ (1%) for samples with $\varepsilon_r = 4.4 - j1.55$ lead to higher relative errors, $|\Delta\varepsilon_r/\varepsilon_r|$ in the predicted relative complex permittivity, reaching up to 4.78%. This discrepancy arises from the relatively low expected value of ε_r. For instance, if the predicted ε_r' value is 4.6, the

percentage change in $|\Delta\varepsilon_r'/\varepsilon_r'|$ becomes $|4.6–4.4|/4.4 \times 100\% = 4.55\%$. On the other hand, for other highly lossy samples, the percentage relative error $|\Delta\Gamma_a/\Gamma_a|$ in measurements closely corresponds to the error introduced in the prediction of ε_r.

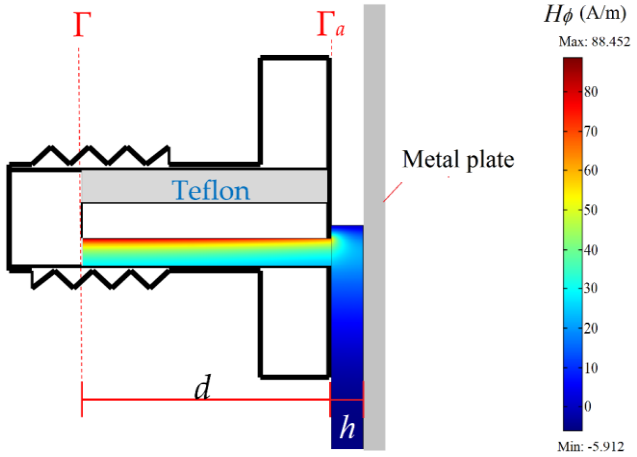

Figure 7 Simulated rotational symmetry half-space simulated magnetic field, $H\phi$ of open-ended coaxial probe with aperture backed by metal plate

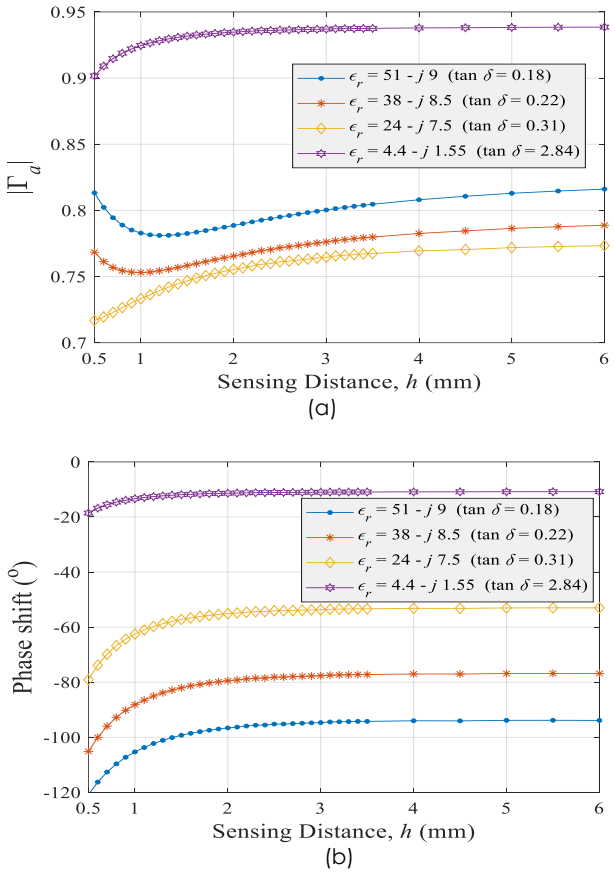

Figure 8 Variation in (a) linear magnitude, $|\Gamma_a|$ and (b) phase shift, ϕ_a with sensing distance, h at 2.45 GHz for four kinds of samples

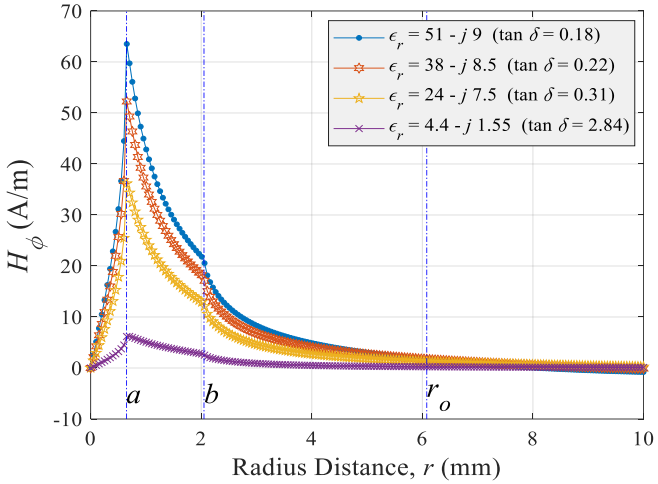

Figure 9 Variation in simulated magnetic field, H_ϕ with radius distance, r at probe aperture for four kinds of samples at 2.45 GHz

2.3 Six-Port CRM Circuit Calibration

In this section, the calibration of the six-port CRM circuit is briefly described. The calibration includes four main purposes as [21, 22]:

1. Ensure that the input RF power, P, from signal generator and measured output voltage, V at each port (port-4, -5, -6, and reference port) complies with the square-law characteristic, namely input RF power, $P \propto$ output DC voltage, V.

2. Correlate the input RF power, P of different power levels (from +10 dBm to -20 dBm with an interval of 1 dBm) with the measured voltage, V_{diode} at ports-4, -5, and -6 to calibrate the nonlinear characteristics of the six-port circuit. The P is expressed as a function of measured voltage, V_{diode} applicable for various types of connected components at the measurement-port (using open-circuit, short-circuit, offset short-circuit, and 50 Ω match load kits):

$$P = (\beta \times V)\exp\left(\sum_{n=0}^{N} \alpha_n V^n\right) \quad (4)$$

Here, β signifies a constant value. Symbol a_n represents the coefficients of the n^{th} order polynomial. The voltage, V in equation (4) is given as:

$$V = \zeta\left(V_{diode} - V_o\right) \quad (5)$$

where ζ denotes the scale factor, ensuring that the values are calibrated to yield a maximum approximate value of 0.5 for V. Additionally, V_o stands for the output voltage of the diode

detector under the condition of zero input power, P = 0 watt. Once parameters of β, a_n, and ζ for each port are determined, the P function in equation (4) is assumed to be the detected output power of the diode detector. The measured power, P at port-4, -5, and -6 are represented by P_4, P_5, and P_6, respectively.

3. Convert the measured powers, P_4, P_5, and P_6 to the unique complex reflection coefficient, R of the six-port circuit:

$$R=\left\{\begin{array}{l}\dfrac{P_4-x_1P_5+x_5}{2\sqrt{x_5}}\\ +j\left[\dfrac{P_4-x_2P_6+u_6^2+v_6^2}{2v_6}-\left(\dfrac{P_4-x_1P_5+x_5}{2v_6\sqrt{x_5}}\right)u_6\right]\end{array}\right\} \quad (6)$$

where

$$u_6=\frac{x_4+x_5-x_3}{2\sqrt{x_5}} \quad \text{and} \quad v_6=\pm\sqrt{x_4-u_6^2}$$

The values of x_1, x_2, x_3, x_4, and x_5 in equation (6) are determined by measuring power values (P_4, P_5, and P_6) of the sliding short kit connected to the measurement port. The sliding short kit's offset position is sequentially adjusted, and the powers (P_{ref}, P_4, P_5, and P_6) are measured at each position to ascertain both the minimum power, P_{min} and the maximum power, P_{max} values at ports-4, -5 and -6, respectively. Up to sixteen offset short positions are measured. Finally, the x_1, x_2, x_3, x_4, and x_5 are estimated as:

$$x_1=\left(\frac{\sqrt{P_{4\,max}}\pm\sqrt{P_{4\,min}}}{\sqrt{P_{6\,max}}\pm\sqrt{P_{6\,min}}}\right)^2 \quad (7a)$$

$$x_2=\left(\frac{\sqrt{P_{4\,max}}\pm\sqrt{P_{4\,min}}}{\sqrt{P_{5\,max}}\pm\sqrt{P_{5\,min}}}\right)^2 \quad (7b)$$

$$x_3=\left[\frac{\left(x_2P_{6\,max}-x_1P_{5\,min}\right)-\left(x_2P_{6\,min}-x_1P_{5\,max}\right)}{2\left(\sqrt{P_{4\,max}}\pm\sqrt{P_{4\,min}}\right)}\right]^2 \quad (7c)$$

$$x_4=\left[\frac{\left(P_{4\,max}-x_2P_{6\,min}\right)-\left(P_{4\,min}-x_2P_{6\,max}\right)}{2\left(\sqrt{P_{4\,max}}\pm\sqrt{P_{4\,min}}\right)}\right]^2 \quad (7d)$$

$$x_5=\left[\frac{\left(x_1P_{5\,max}-P_{4\,min}\right)-\left(x_1P_{5\,min}-P_{4\,max}\right)}{2\left(\sqrt{P_{4\,max}}\pm\sqrt{P_{4\,min}}\right)}\right]^2 \quad (7e)$$

4. Calibrate the complex reflection coefficient, Γ at measurement-port from the unique complex reflection coefficient, R [equation (6)] as[23]:

$$\Gamma=\frac{R-\gamma_1}{\gamma_2R+\gamma_3} \quad (8)$$

Here, γ_1, γ_2, and γ_3 presents the complex coefficients determined using open-circuit, short-circuit, and match-load standards. The γ_1, γ_2, and γ_3 can be determined as:

$$\gamma_1=R_{load} \quad (9a)$$

$$\gamma_2=\frac{R_{short}+R_{open}-2R_{load}}{R_{short}-R_{open}} \quad (9b)$$

$$\gamma_3=\frac{R_{open}R_{load}+R_{short}R_{load}-2R_{open}R_{short}}{R_{short}-R_{open}} \quad (9c)$$

where R_{open}, R_{short}, and R_{load} denote the measured unique reflection coefficients of the open-circuit, short-circuit, and match-load standards connected at measurement-port, respectively.

2.4 Coaxial Probe Calibration

Given the quasi-TEM mode assumption, the complex reflection coefficient, Γ of the coaxial probe connected at plane BB' (the measurement port), depicted in Figure 6(c), is de-embedded to the aperture probe at plane AA'. This process yields a calibrated reflection coefficient, Γ_a at aperture probe using exponential term of $\exp(2jk_cz)$ as (See Figure 10) [20]:

$$\Gamma_a=\Gamma\exp\left(2jk_cz\right) \quad (10)$$

symbols z and k_c = $(2\pi f/c)\sqrt{\varepsilon_c}$ denote the apparent coaxial length (in meters) and the propagation constant of the coaxial line, respectively. Here, f, c and ε_c represent the operating frequency (in Hz), speed of light in free space (299792458 ms^{-1}), and the relative dielectric constant for the material filling the coaxial line (Teflon: ε_c = 2.06), respectively. The complex values of z in equation (10) takes into account aperture fringing effect.

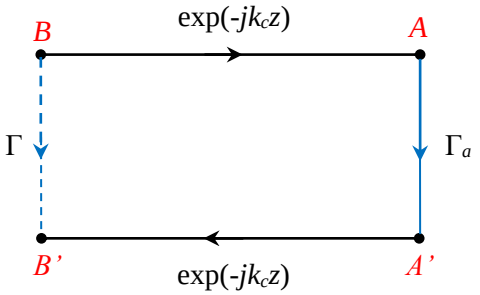

Figure 10 De-embedded one-port network

In the de-embedding procedure, reflection coefficient measurements, Γ_{Air} are taken for air at the plane *BB'*. Then, standard values for the air reflection coefficient, Γ_{a_Air} at the plane *AA'* are simulated using COMSOL Multiphysics software. Once both values (Γ_{Air} and Γ_{a_Air}) are acquired, the apparent coaxial length, z can be determined as:

$$z = \left(\frac{-j}{2k_c}\right)\ln\left(\frac{\Gamma_{a\_Air}}{\Gamma_{Air}}\right) = z' + jz'' \tag{11}$$

At the same time, the attenuation constant, α (in Np/m) in the coaxial line of the proble can be derived from the apparent coaxial length, $z = z' + jz''$ as:

$$\alpha = \left(\frac{2\pi f}{c}\right)\left|\frac{z''}{z'}\right| \tag{12}$$

The real part of apparent coaxial length, z' versus operation frequency, *f* is plotted in Figure 11 (a). From calculation using equation (11), the apparent length, z has been lengthened by 2 % compared with actual physical dimension length (*d* = 7.6 mm) up to 6.5 GHz, which is caused by an aperture fringing field. The attenuation constant, α increase with the frequency, *f* is plotted in Figure 11 (b) which the relationship between α and *f* is given as $\alpha \approx 0.1 \times 10^{-9} f$.

Finally, the apparent complex length, z of the coaxial probe and the measured complex reflection coefficient, Γ at *BB'* are inserted into equation (13) in order to predict the relative complex permittivity, ε_r of the sample terminated at *AA'* (aperture probe) as [24]:

$$\varepsilon_r = \left(\frac{Y_o}{j\omega C_o}\right)\left\{\frac{1-\Gamma\exp(2jk_c z)}{1+\Gamma\exp(2jk_c z)}\right\} \tag{13}$$

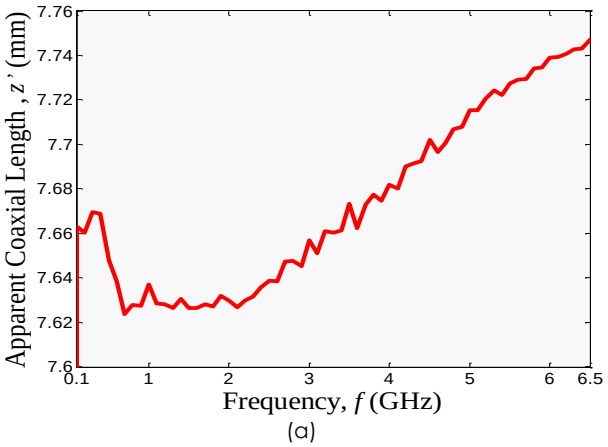

(a)

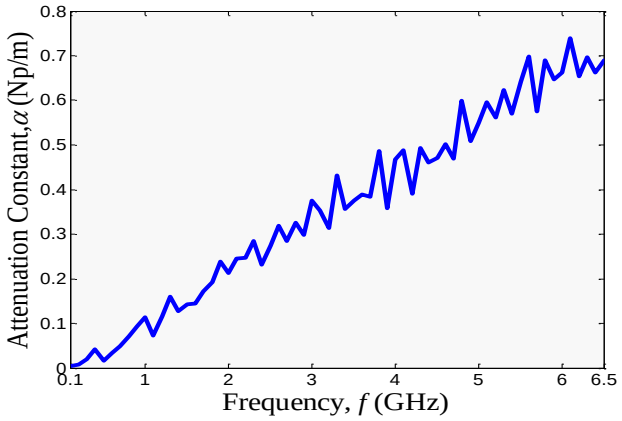

(b)

Figure 11 Variation in (a) apparent coaxial length, z' and (b) attenuation constant, α with frequency, *f*

2.5 Synthetic Breast Tissues

The synthetic breast tissue samples are produced according to the method outlined by [21, 25], utilizing solutions composed of pure water and Triton TX-100 in varying volume ratios as detailed in Table 2.

Table 2 Synthetic breast specimens comprising various proportions of water and Triton TX-100

	Category	TX-100 (% vol.)	Water (% vol.)
T	Tumour	20	80
B1	Fibroglandular 2	30	70
B2	Fibroglandular 1	40	60
B3	Fatty/adipose	100	0

The specific volume ratios from Table 2 are measured using a volumetric burette. Subsequently, the measured volumes of the TX-100 solution and water are combined and thoroughly mixed in a cylindrical flask. The solution labeled *T* represents the tumor breast tissue, while solutions *B1*, *B2*, and *B3* correspond to three types of normal breast tissues, respectively. Samples *T* and *B1* are prepared under ambient conditions, whereas sample *B2* is processed at 60°C due to its elevated viscosity, making stirring challenging at room temperature.

3.0 RESULTS AND DISCUSSION

The functionality of the six-port reflectometer-sensor system (SPR-sensor system) is evaluated through testing and analysis, focusing on the measured reflection coefficient, Γ_a and predicted relative permittivity, ε_r of synthetic breast tissue. Reference values were obtained from the E5071C network analyzer (VNA) and the 85070E dielectric probe which are manufactured by Keysight Technologies Inc.. Additionally, the accuracy and precision of measurements obtained from the study SPR-sensor

system are compared to those from a previous five-port ring reflectometer-sensor system (FPR-sensor system) [21]. Also, the linear magnitude, $|\Gamma_a|$ and phase shift, ϕ_a of the reflection coefficient for breast tissue samples are measured using both the study SPR-sensor system and the E5071C VNA with 85070E dielectric probe for comparison, as depicted in Figure 12 and Figure 13. Notably, the measured $|\Gamma_a|$ (indicated by the black dashed line) utilizing the SPR-sensor system displays ripple/noise characteristics, which are addressed by employing a first-order polynomial local regression (LOESS) model with a span of 0.15. Figure 12 and Figure 13 shows the resultant smoothed $|\Gamma_a|$ and ϕ_a which are depicted by the red circled line. It is evident that compared to the $|\Gamma_a|$ measurement, the sensitivity of the ϕ_a measurement for *T*, *B*1, *B*2, and *B*3 is significantly greater. Typically, the range of regular ϕ_a measurement is from -180° to 180°, whereas the range of linear magnitude, $|\Gamma_a|$ measurement of the reflection coefficient is only from 0 to 1. Consequently, the uncertainty in $|\Gamma_a|$ measurement is relatively higher than ϕ_a measurement. Clearly, ϕ_a measurement is effectively utilized to distinguish between tumor and normal breast tissues.

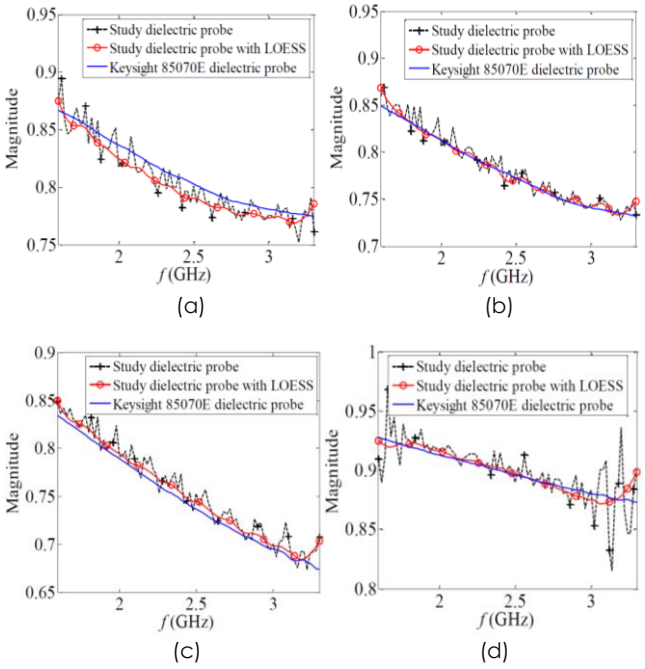

Figure 12 The calibrated magnitude of $|\Gamma_a|$ of (a) *T*, (b) *B*1, (c) *B*2, and (d) *B*3, respectively

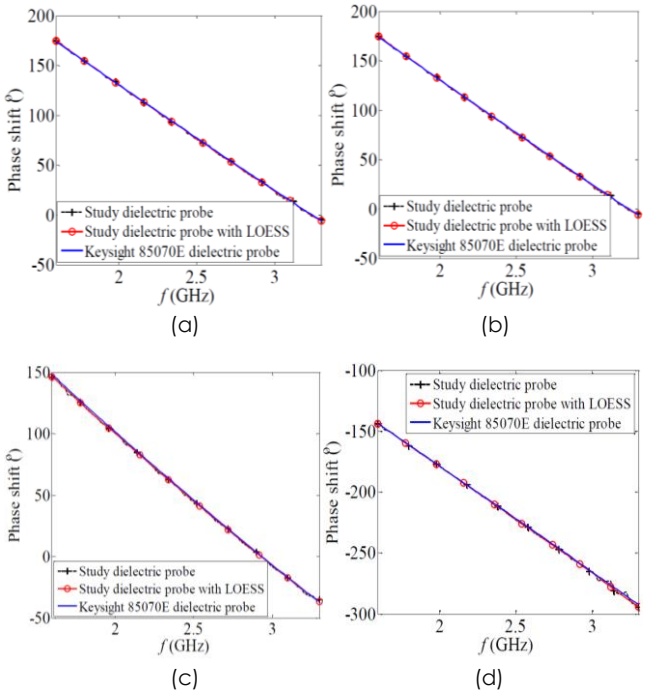

Figure 13 The calibrated phase shift, ϕ_a of (a) T, (b) B1, (c) B2, and (d) B3, respectively

The uncertainty analysis of Γ_a *in vitro* measurements by both the previous FPR-sensor literature [21] and the study SPR-sensor system. Absolute errors are determined using measurements from the E5071C VNA with 85070E dielectric probe. Results indicate that the SPR-sensor system offers superior accuracy and wider bandwidth coverage (from 1.5 GHz to 3.3 GHz) compared to the FPR-sensor system [21]. Maximum mean absolute errors for magnitude, $\Delta|\Gamma_a|$ and phase, $\Delta\phi_a$ measurements with the SPR-sensor system are 0.011 and 1.22°, respectively, lower than those of the FPR-sensor system [21] with $\Delta|\Gamma_a| = 0.03$ and $\Delta\phi_a = 3.6°$. The measurement error of Γ_a with the SPR system is nearly three times smaller than that of the FPR system [21]. The overall maximum and mean absolute errors in Γ_a measurements from 1.5 GHz to 3.3 GHz using SPR-sensor system are presented in Table 3.

Table 3 Maximum and mean absolute errors in Γ_a

	Filter (LOESS)	Absolute Error			
		Maximum		Mean	
		$\Delta\|\Gamma_a\|$	$\Delta\phi_a$ (°)	$\Delta\|\Gamma_a\|$	$\Delta\phi_a$ (°)
T	Yes	0.015	1.92	0.0092	1.07
	No	0.029	4.56	0.0092	1.22
*B*1	Yes	0.014	1.29	0.0027	0.84
	No	0.017	3.31	0.0068	0.96
*B*2	Yes	0.029	0.95	0.0069	0.45
	No	0.034	2.50	0.0113	0.78
*B*3	Yes	0.026	1.78	0.0033	0.66
	No	0.061	3.97	0.0109	0.85

On the other hand, the ε_r (= $\varepsilon_r' - j\varepsilon_r''$) values of the breast tissue are derived from the measured reflection coefficient, Γ_a using equation (13). Comprising both the real part, ε_r' and imaginary part, ε_r'' represents the dielectric constant and loss factor, respectively. Figures 14 and 15 illustrate the predicted ε_r' and ε_r'' values, derived from the LOESS-treated linear magnitude and phase shift of the Γ_a. Additionally, measurements of ε_r' and ε_r'' obtained by the E5071C VNA with 85070E dielectric probe serve as benchmarks for comparison with those predicted by the study SPR-sensor system. Despite LOESS treatment, some ripple/noise persists in the predicted ε_r' and ε_r'' values, necessitating further LOESS application to refine them. Observing Figures 14 and 15, synthetic breast tissue samples of tumor, *T* exhibit the highest ε_r' and ε_r'' values, while sample *B*3 demonstrates the lowest. The elevated ε_r' and ε_r'' values in the *T* sample are attributed to its high water content, whereas *B*3, lacking water, displays the lowest values. For instance, the dielectric constant, ε_r' values at 2.45 GHz for *T* and *B*1 samples range from 50.94 to 51.49 and 37.80 to 39.02, respectively. These findings suggest that *in vitro* measurements of ε_r' can effectively distinguish between tumor and normal breast tissues, as normal tissue typically exhibits $\varepsilon_r' < 50$, while tumor tissue shows $\varepsilon_r' > 50$. Table 4 lists the uncertainties in the predicted ε_r' and ε_r'' of the synthetic breast samples from 1.5 GHz to 3.3 GHz, with and without LOESS filter treatments. The mean absolute error (MAE) for ε_r' ranges from 0.2 to 1.3 across all four synthetic breast tissue samples (*T*, *B*1, *B*2, and *B*3). Meanwhile, the MAE for ε_r'' falls between 0.07 and 0.75.

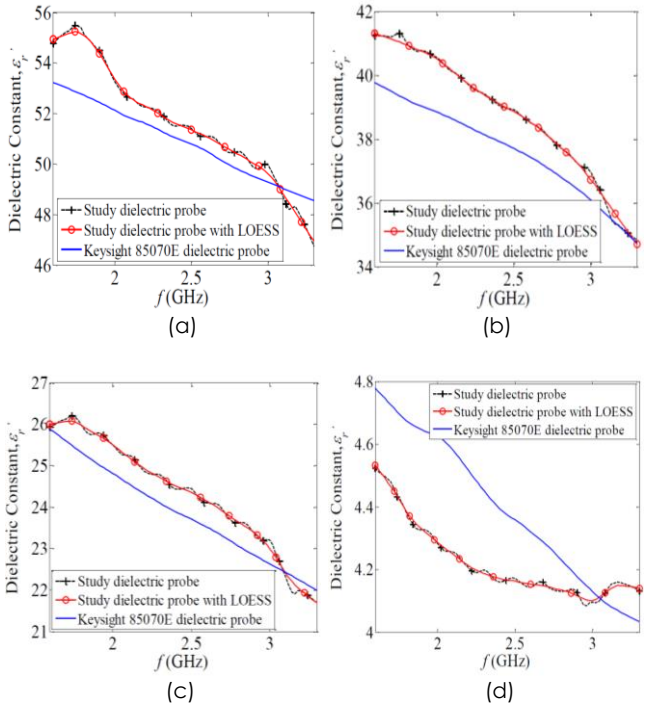

Figure 14 The predicted ε_r' for the (a) *T*, (b) *B*1, (c) *B*2, and (d) *B*3 of the synthetic breast tissues

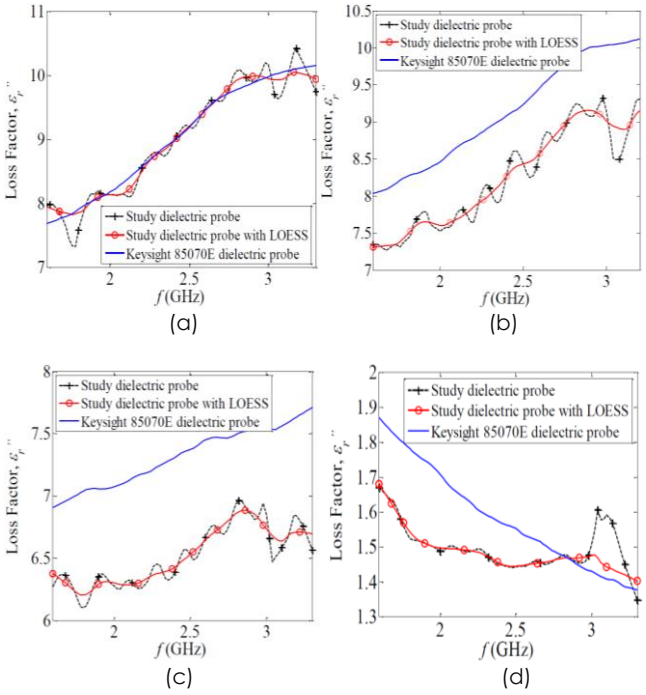

Figure 15 The predicted ε_r'' for the (a) *T*, (b) *B*1, (c) *B*2, and (d) *B*3 of the synthetic breast tissues

Table 4 Maximum and mean absolute errors in ε_r

	Filter (LOESS)	Absolute Error			
		Maximum		Mean	
		$\Delta\ \varepsilon_r'$	$\Delta\ \varepsilon_r''$	$\Delta\ \varepsilon_r'$	$\Delta\ \varepsilon_r''$
T	Yes	2.21	0.27	0.88	0.07
	No	2.43	0.57	0.92	0.14
*B*1	Yes	1.73	0.93	1.19	0.75
	No	1.95	1.16	1.30	0.75
*B*2	Yes	0.71	1.04	0.53	0.75
	No	0.79	1.20	0.54	0.75
*B*3	Yes	0.34	0.24	0.20	0.11
	No	0.38	0.26	0.20	0.13

4.0 CONCLUSION

The developed six-port reflectometry (SPR) system shows promise in predicting the ε_r of tumor and normal breast tissue. While the calibration procedure and use of a coaxial probe have produced favorable results in measuring dielectric properties across a broad frequency range, discrepancies were noted compared to a commercial vector network analyzer (VNA). Maximum absolute errors raise concerns about the system's accuracy, particularly in distinguishing between normal and tumor tissue. Further validation studies with clinical samples and rigorous error analysis are needed to assess the SPR system's clinical utility and reliability in medical diagnostics. These further studies should involve a large and diverse set of clinical tissue samples to ensure the system's accuracy and robustness in real-world conditions.

Acknowledgement

This research received full support from Universiti Teknologi Malaysia through the UTM Fundamental Research Grant (Q.J130000.3851.22H13). The authors also extend their gratitude to Dr. Lee Chia Yew for their invaluable assistance.

Conflicts of Interest

The author(s) declare(s) that there is no conflict of interest regarding the publication of this paper.

References

[1] Siegel, R. L., Giaquinto, A. N. and Jemal, A. 2024. Cancer Statistics, 2024. *CA: A Cancer Journal for Clinicians*. 74(1): 12–49.
Doi: 10.3322/caac.21820.

[2] Baran, A., Kurrant, D., Zakaria, A., Fear, E., LoVetri, J. 2014. Breast Cancer Imaging Using Microwave Tomography with Radar-Derived Prior Information. *2014 USNC-URSI Radio Science Meeting*.
Doi: 10.1109/USNC-URSI.2014.6955642.

[3] Bicer, M. B. 2023. Radar-Based Microwave Breast Imaging Using Neurocomputational Models. *Diagnostics*. 13(5): 930.
Doi: 10.3390/diagnostics13050930.

[4] Wang, L. L. 2023. Microwave Imaging and Sensing Techniques for Breast Cancer Detection. *Micromachines*. 14(7): 1462.
Doi: 10.3390/mi14071462.

[5] Hossain, T. M., Jamlos, M. F., Jamlos, M. A., Dzaharudin, F., Ismail, M. Y., Al-Bawri, S. S., Sugumaran, S., Ahmad Salimi, M. N. 2020. Bandwidth Enhancement of Five-Port Reflectometer-Based ENG DSRR Metamaterial for Microwave Imaging Application. *Sensors and Actuators A: Physical*. 303: 111638.
Doi: 10.1016/j.sna.2019.111638.

[6] Marie Mertens, Maede Chavoshi, Olivia Peytral-Rieu, Katia Grenier, Dominique Schreurs. 2013. Dielectric Spectroscopy: Revealing the True Colors of Biological Matter. *IEEE Microwave Magazine*. 24(4): 49–62.
Doi: 10.1109/MMM.2022.3233510.

[7] Champbell, A. M. and Land, D. V. 1992. Dielectric Properties of Female Human Breast Tissue Measured In Vitro at 3.2 GHz. *Physics in Medicine & Biology*. 37(1): 193–210.
Doi: 10.1088/0031-9155/37/1/014.

[8] Cheng, Y. and Fu, M. H. 2018. Dielectric Properties for Non-Invasive Detection of Normal, Benign, and Malignant Breast Tissues using Microwave Theories. *Thorac Cancer*. 9(4): 459–465.
Doi: 10.1111/1759-7714.12605.

[9] Jordan Krenkevich, Gabrielle Fontaine, Evelyne Hluszok, Tyson Reimer, Stephen Pistorius. 2024. Tissue Mimicking Materials for Shell-Based Phantoms in Breast Microwave Sensing. *IEEE Journal of Electromagnetics, RF, and Microwaves in Medicine and Biology*. 8(3): 213–219.
Doi: 10.1109/JERM.2024.3379747.

[10] Simona Di Meo, Alessia Cannatà, Carolina Blanco-Angulo, Giulia Matrone, Andrea Martínez-Lozano, Julia Arias-Rodríguez, José M. Sabater-Navarro, Roberto Gutiérrez-Mazón, Héctor García-Martínez, Ernesto Ávila-Navarro, Marco Pasian. 2024. Multi-Layer Tissue-Mimicking Breast Phantoms for Microwave-Based Imaging Systems. *IEEE Journal of Electromagnetics, RF, and Microwaves in Medicine and Biology*.
Doi: 10.1109/JERM.2024.3379750.

[11] Mousa Hussein, Falah Awwad, Dwija Jithin, Husain El Hasasna, Khawlah Athamneh, Rabah Iratni. 2019. Breast Cancer Cells Exhibits Specific Dielectric Signature *In Vitro* Using the Open-Ended Coaxial Probe Technique from 200 MHz to 13.6 GHz. *Scientific Reports*. 9: 4681.
Doi: 10.1038/s41598-019-41124-1.

[12] Lena Kranold, Jasmine Boparai, Leonardo Fortaleza, Milica Popović. 2022. Skin Phantoms for Microwave Breast Cancer Detection: A Comparative Study. *IEEE Journal of Electromagnetics, RF, and Microwaves in Medicine and Biology*. 6(2): 175 – 181.
Doi: 10.1109/JERM.2021.3084126.

[13] Jordan Krenkevich, Gabrielle Fontaine, Tyson Reimer, Stephen Pistorius. 2023. Improved Tissue Mimicking Materials for Shell-Based Phantoms in Breast Microwave Sensing. In: IEEE MTT-S International Microwave Biomedical Conference (IMBioC), pp. 46 – 48.
Doi: 10.1109/IMBioC56839.2023.10305107.

[14] Nural Pastaci Ozsobaci, Emre Onemli, Cemanur Aydinalp, Tuba Yilmaz. 2024. Measurement and Analysis of In Vivo Microwave Dielectric Properties Collected From Normal, Benign, and Malignant Rat Breast Tissues: Classification Using Supervised Machine Learning Algorithms. *IEEE Transactions on Instrumentation and Measurement*. 73: 4006911.
Doi: 10.1109/TIM.2024.3390692.

[15] Canicattì, E., Sánchez-Bayuela, D. Á., Castellano, C. R., Angulo, P. M. A., González, R. G., Cruz Hernández, L. M., Martín, J. R., Tiberi, G. and Monorchio, A. 2023. Dielectric Characterization of Breast Biopsied Tissues as Pre-Pathological Aid in Early Cancer Detection: A Blinded Feasibility Study. *Diagnostics*. 13(18): 3015.
Doi: 10.3390/diagnostics13183015.

[16] Fernández-Aranzamendi, E. G., Castillo-Araníbar, P. R., Román Castillo, E. G. S., Oller, B. S., Ventura-Zaa, L., Eguiluz-Rodriguez, G., González-Posadas, V. and Segovia-Vargas, D. 2024. Dielectric Characterization of Ex-Vivo Breast Tissues: Differentiation of Tumor Types through Permittivity Measurements. *Cancers* 16(4): 793.
Doi: 10.3390/cancers16040793.

[17] Simona Di Meo, Giulia Matrone, Giovanni Magenes, Marco Pasian. 2024. On the Low-Cost Production of Tissue-Mimicking Skin Phantoms Up to 40 GHz. *IEEE Journal of Electromagnetics, RF, and Microwaves in Medicine and Biology*. 8(1): 51–58.
Doi: 10.1109/JERM.2024.3349851.

[18] Nadera, N., You, K. Y., Dimon, M. N. and Khamis, N. H. 2018. Wideband and Compact Wilkinson Power Divider Utilizing Series Delta-Stub and Folded Stepped-Impedance Transmission Line. *Radioengineering*. 27(1): 200–206.
Doi: 10.13164/re.2018.0200.

[19] Nadera, N. and You, K. Y. 2018. Broadband and Compact Complex Ratio Measuring Unit. *Microwave and Optical Technology Letters*. 60(12): 3039–3045.
Doi: 10.1002/mop.31445.

[20] You, K. Y. 2016. RF Coaxial Slot Radiators: Modeling, Measurements, and Applications. Artech House, Norwood, MA, U.S..

[21] Lee, C. Y., You, K. Y., Abbas, Z., Lee, K. Y., Lee, Y. S. and Cheng, E. M. 2018. S-Band Five-Port Ring Reflectometer-Probe System for In Vitro Breast Tumor Detection. *International Journal of RF and Microwave Computer-Aided Engineering.* 28(3): e21198.
Doi: 10.1002/mmce.21198.

[22] Staszek, K. 2024. Fully Analytical Approach to Calibration of Six-Port Reflectometers Using Matched Load and Unknown Loads for One-Port Measurements. *IEEE Transactions on Microwave Theory and Techniques*. 72(1): 183–193.
Doi: 10.1109/TMTT.2023.3291758.

[23] Lin, W. G. and Ruan, C. L. 1989. Measurement and Calibration of a Universal Six-Port Network Analyzer. *IEEE Transactions on Microwave Theory and Techniques*. 37(4): 734–742.
Doi: 10.1109/22.18847.

[24] You, K. Y. and Sim, M. S. 2018. Precision Permittivity Measurement for Low-Loss Thin Planar Materials Using Large Coaxial Probe from 1 to 400 MHz. *Journal of Manufacturing and Materials Processing*. 2(4): 81. Doi: 10.3390/jmmp2040081.
[25] Romeo, S., Di Donato, L., Bucci, O. M., Catapano, I., Crocco, L., Scarfì, M. R. and Massa, R. 2011. Dielectric Characterization Study of Liquid-Based Materials for Mimicking Breast Tissues. *Microwave and Optical Technology Letters*. 53(6): 1276–1280. Doi: 10.1002/mop.26001.